

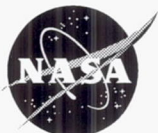
E9849
7-5-96

**NASA
Technical
Paper
3576**

June 1996

**Experimental Performance of a High-
Area-Ratio Rocket Nozzle at High
Combustion Chamber Pressure**

Robert S. Jankovsky,
John M. Kazaroff,
and Albert J. Pavli



National Aeronautics and
Space Administration

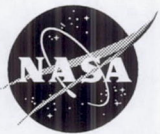
**NASA
Technical
Paper
3576**

1996

**Experimental Performance of a High-
Area-Ratio Rocket Nozzle at High
Combustion Chamber Pressure**

Robert S. Jankovsky
and John M. Kazaroff
*Lewis Research Center
Cleveland, Ohio*

Albert J. Pavli
*NYMA, Inc.
Brook Park, Ohio*



National Aeronautics and
Space Administration
Office of Management
Scientific and Technical
Information Program

Experimental Performance of a High-Area-Ratio Rocket Nozzle at High Combustion Chamber Pressure

Robert S. Jankovsky, John M. Kazaroff, and Albert J. Pavli
National Aeronautics and Space Administration
Lewis Research Center
Cleveland, Ohio

Summary

An experimental investigation was conducted to determine the thrust coefficient of a high-area-ratio rocket nozzle at combustion chamber pressures of 12.4 to 16.5 MPa (1800 to 2400 psia). A nozzle with a modified Rao contour and an expansion area ratio of 1025:1 was tested with hydrogen and oxygen at altitude conditions. The same nozzle, truncated to an area ratio of 440:1, was also tested. Values of thrust coefficient are presented along with characteristic exhaust velocity efficiencies, nozzle wall temperatures, and overall thruster specific impulse.

Introduction

The design of high-area-ratio rocket nozzles requires knowledge of core flow, boundary layer interaction, contour effects, supersonic shock effects, and wall heat transfer effects. Experimentally these effects are difficult, if not impossible, to individually quantify. Their combined effects, though, can be accounted for in an overall nozzle performance or thrust coefficient C_F , which can be calculated from thrust and chamber pressure. Even the parameter C_F has been difficult to obtain experimentally because altitude test facilities for nozzles with area ratios in the range of 700 to 1000 are not available. Therefore, a nozzle designer primarily uses theoretical methods incorporated in numerical codes. These codes are considered validated (ref. 1) for low-area-ratio nozzles and are being used to extrapolate to high-area-ratio nozzles. Without experimental validation, confidence in these extrapolations is lacking and questions as to the relevance of trades studies for future rocket engines are raised. Hence, an experimental program was undertaken to obtain the C_F for a high-area-ratio nozzle so that nozzle performance codes could be validated in this regime. As part of this program, a series of tests were conducted in the altitude test capsule at the NASA Lewis Rocket Engine Test Facility (RETF). Previous tests in this program were in the laminar boundary layer regime (refs. 2 to 4) at a nominal combustion chamber pressure of 2.4 MPa (350 psia) and at Reynolds num-

bers (based on throat diameter) from 3.11 to 4.14×10^5 . This report presents values of the thrust coefficient C_F , characteristic exhaust velocity efficiency ηC^* , nozzle wall temperature, and overall thruster specific impulse $I_{sp,V}$ for a 1025:1-area-ratio nozzle at combustion chamber pressures from 12.4 to 16.5 MPa (1800 to 2400 psia) and throat Reynolds numbers from 1.43 to 2.05×10^6 . These tests were considered to be in the turbulent boundary layer regime (ref. 5). The nozzles used in these tests had a nominal 2.54-cm-(1-in.-) diameter throat with area ratios of 1025:1 and 440:1 and were fired with hydrogen and oxygen.

Symbols

A_{ex}	nozzle exit area, cm^2 (in.^2)
A_t	nozzle throat area, cm^2 (in.^2)
A_v	venturi throat area, cm^2 (in.^2)
C_d	venturi discharge coefficient, dimensionless
C_F	thrust coefficient, dimensionless
$C_{F,V}$	vacuum thrust coefficient, dimensionless
$C_{F,V,Th(ODE)}$	theoretical, one-dimensional-equilibrium (ODE) vacuum thrust coefficient (obtained from Chemical Equilibrium Composition (CEC) program, ref. 6), dimensionless
$C_{F,V,Th(TDK)}$	theoretical, two-dimensional-kinetics (TDK) vacuum thrust coefficient (obtained from ref. 7), dimensionless
C^*	characteristic exhaust velocity, m/s (ft/s)
$C_{Th(ODE)}^*$	theoretical, one-dimensional-equilibrium characteristic exhaust velocity (obtained from CEC program, ref. 6), m/s (ft/s)

F	thrust (corrected for aneroid effect), N (lb _f)	V	velocity through venturi throat, m/s (in./s)
F_V	vacuum thrust (experimentally measured thrust corrected to vacuum conditions), N (lb _f)	V_{av}	mass-averaged injection velocity of propellants, m/s (ft/s)
g	acceleration of gravity, 9.807 m/s ² (32.174 ft/s ²)	ϵ	nozzle exit expansion area ratio, A_{ex}/A_t , dimensionless
g_c	proportionality constant, 1 kg-m/N-s ² (32.2 lb _m -ft/lb _f -s ²)	ϵ_c	thruster contraction area ratio, dimensionless
I	theoretical subsonic specific impulse inside combustion chamber (obtained from CEC program, ref. 6), N-s/kg (lb _f -s/lb _m)	ηC^*	characteristic exhaust velocity efficiency, percent
$I_{sp,V}$	vacuum specific impulse, N-s/kg (lb _f -s/lb _m)	$\eta C_{F,V}$	vacuum thrust coefficient efficiency, percent
$I_{sp,V,Th(ODE)}$	theoretical, one-dimensional-equilibrium vacuum specific impulse (obtained from CEC program, ref. 6), N-s/kg (lb _f -s/lb _m)	$\eta I_{sp,V}$	vacuum specific impulse efficiency, percent
\dot{m}	propellant mass flow rate, kg/s (lb _m /s)	ρ	fluid density, kg/m ³ (lb _m /in. ³)
O/F	propellant mixture ratio (oxidizer flow divided by fuel flow), dimensionless	σ	standard deviation, dimensionless
P_a	ambient pressure in test capsule, kPa (psia)	<h2>Facility</h2> <p>The facility consisted of an altitude test capsule, a thrust stand, a propellant feed system, and a data acquisition system. The altitude test capsule (fig. 1) simulated the static pressure at altitude by three methods of vacuum pumping: the first, a second-throat diffuser, utilized the kinetic energy of the rocket exhaust to pump the nozzle flow into a spray cooler; the second chilled the exhaust gas in the spray cooler where approximately half was condensed to liquid water and was drained; the third pumped the remaining uncondensed exhaust by nitrogen-driven ejectors. Additional facility details are given in reference 2.</p> <p>The thrust stand had a full-scale measurement range of 17.8 kN (4000 lb_f) and was designed to have a 2-σ variation of less than ± 0.1 percent of full scale. With the test capsule at altitude pressure, the thrust stand was calibrated against a reference load cell, which had a 2-σ variation of less than ± 0.05 percent of full scale and a calibration traceable to the National Institute of Standards and Technology.</p> <p>The propellant feed system consisted of a gaseous hydrogen fuel circuit and a liquid oxygen oxidizer circuit. High-pressure gaseous hydrogen bottles comprised the fuel circuit; the oxidizer circuit was a high-pressure liquid oxygen tank pressurized from high-pressure gaseous helium bottles (fig. 2). The flow rates were measured with calibrated venturis.</p> <p>The data acquisition system consisted of instrumentation (fig. 2), a data digitizer, and a high-speed computer.</p>	
$P_{c,a}$	static pressure at injector end of combustion chamber, MPa (psia)		
$P_{c,e}$	effective combustion chamber total pressure at nozzle entrance, MPa (psia)		
$P_{c,T}$	combustion chamber total pressure after combustion ($P_{c,a}$ corrected for momentum pressure loss), MPa (psia)		
P_{fi}	fuel injection pressure, MPa (psia)		
P_{oi}	oxidizer injection pressure, MPa (psia)		
P_s	static pressure in nozzle, kPa (psia)		
P_s/P_T	static-to-total pressure ratio in combustion chamber (obtained from CEC program, ref. 6), dimensionless		
ΔP	nominal pressure drop, kPa (psia)		
T_{fi}	fuel injection temperature, K (R)		
T_{oi}	oxidizer injection temperature, K (R)		

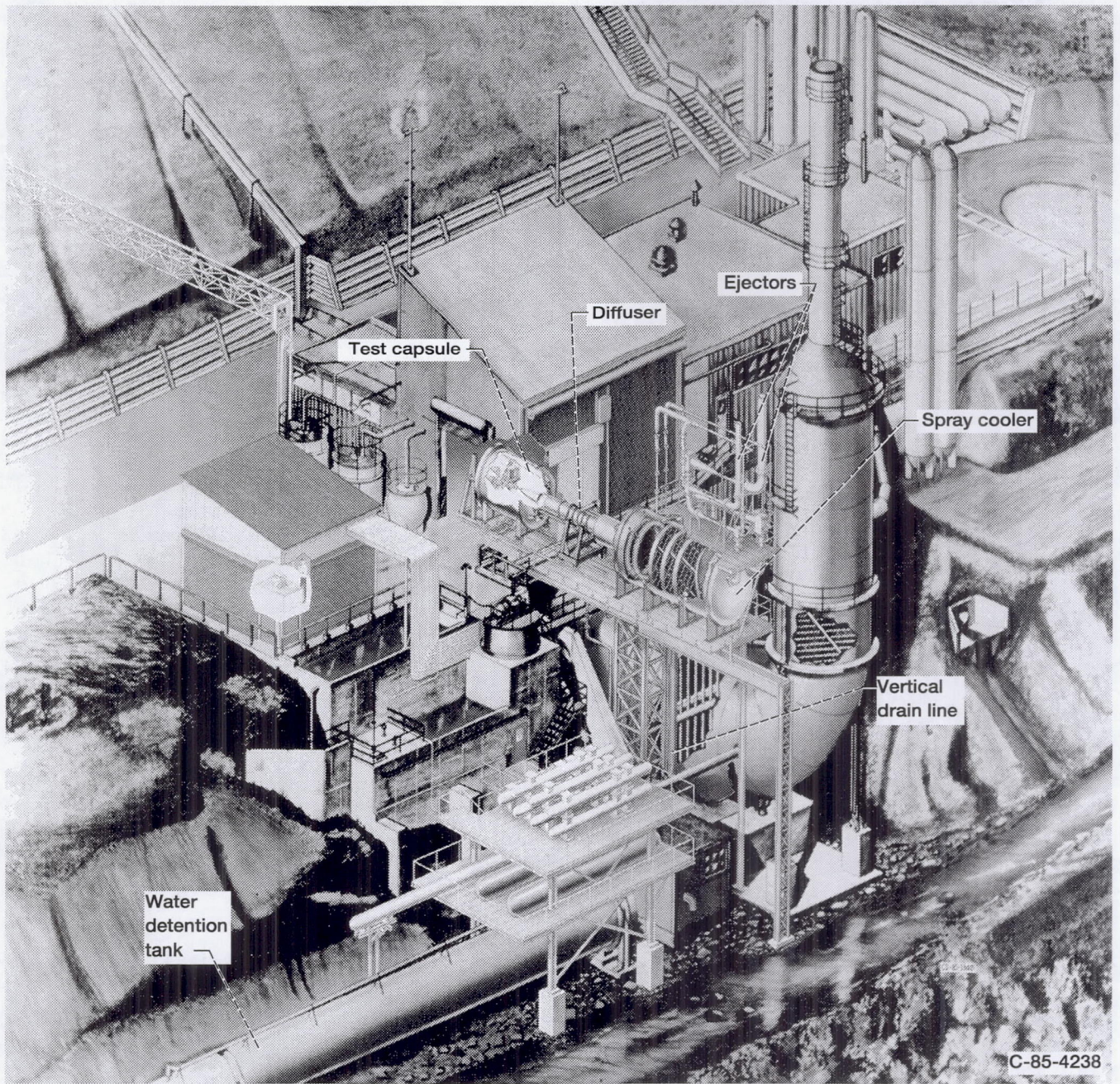


Figure 1.—NASA Lewis Research Center Rocket Engine Test Facility.

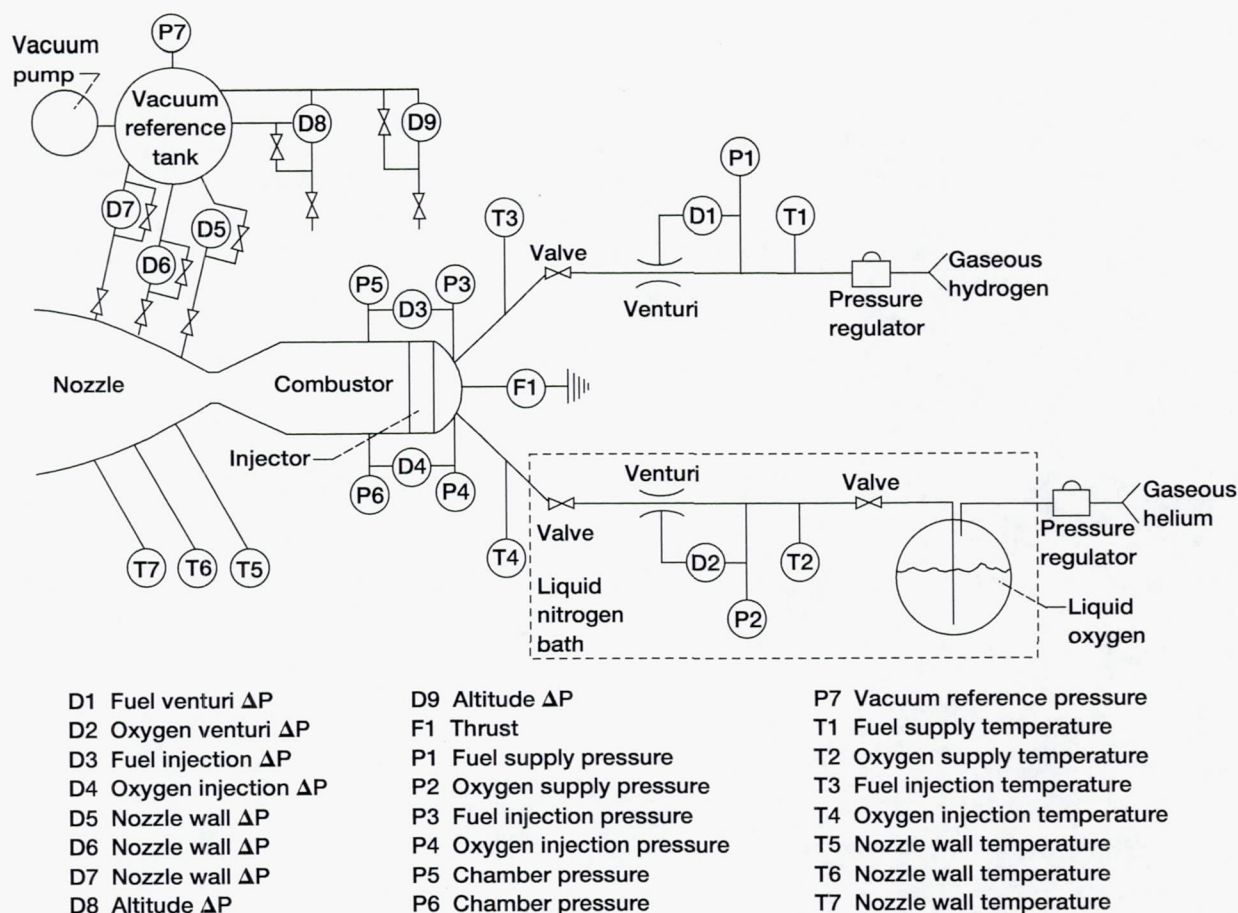


Figure 2.—Propellant system and instrumentation.

Test Hardware

The test hardware were an injector, a combustion chamber, and four nozzles. The injector had a porous face plate for gaseous hydrogen injection and 36 tubes for liquid oxygen injection. A gaseous hydrogen and gaseous oxygen torch ignitor located in the center of the injector ignited the propellant mixture. The injector details are shown in figure 3.

The copper combustion chamber (fig. 4) was water-cooled and had the same contour as the nozzle of reference 2.

Two of the nozzles had a low-area-ratio configuration and two had a high-area-ratio configuration. The two low-area-ratio nozzles ($\epsilon = 10.7:1$ and $4:1$) were used to calibrate the effective combustion chamber pressure at the nozzle entrance $P_{c,e}$ as a function of the static pressure at the end of the combustion chamber $P_{c,a}$. The two high-area-ratio nozzles, $\epsilon = 1025:1$ (fig. 5) and $440:1$, were used to obtain research data. Contour coordinates of the research nozzles are presented in figure 6. The design process that produced the contours is described in reference 2.

	Gaseous hydrogen	Liquid oxygen
Number of holes	-----	36
Hole diameter, cm (in.)	-----	0.119 (0.047)
For pressure drop	-----	0.239 (0.094)
For injection velocity	-----	0.239 (0.094)
Nominal flow rate, \dot{m} , kg/s (lb _m /s)	0.5325 (1.174)	2.389 (5.267)
Nominal pressure drop, ΔP , MPa (psia)	3.777 (547.8)	1.618 (234.7)

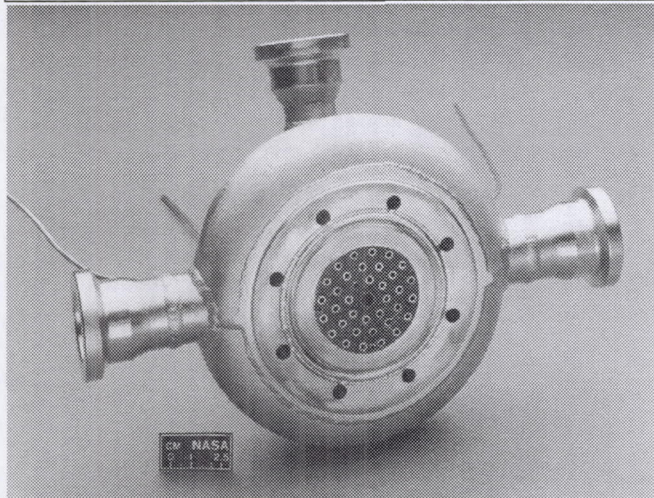


Figure 3.—Test injector.

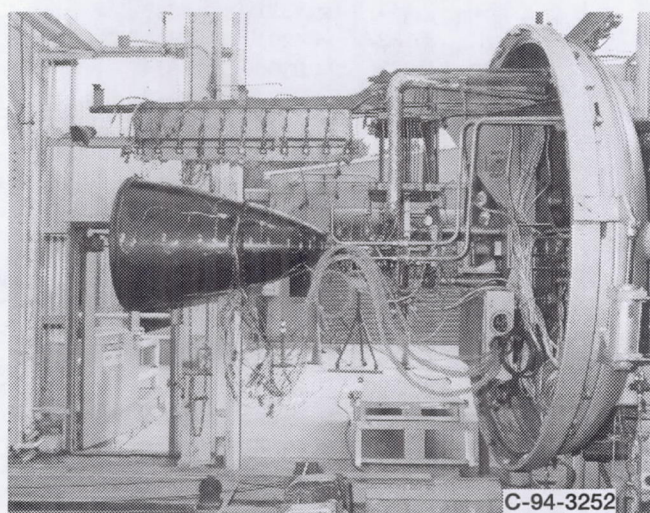


Figure 5.—High-area-ratio nozzle ($\epsilon = 1025:1$).

Procedure

Tests were performed at atmospheric and altitude pressure conditions.

Atmospheric Pressure Tests

Atmospheric pressure tests were first performed to determine $P_{c,e}$. The two low-area-ratio nozzles ($\epsilon = 10.7:1$ and $4:1$) were used in these tests. The firings were approximately 3 s in duration. A steady-state condition was reached at or before 2.5 s, providing about 0.5 s of steady-state operation before shutdown.

Altitude Tests

The high-area-ratio nozzles (1025:1 and 440:1) were tested at altitude. A typical altitude firing started with the gaseous nitrogen ejectors evacuating the test capsule and spray cooler to a pressure of approximately 4.1 kPa (0.6 psia). At this pressure, the thruster was fired for about 3 s. The pumping action during firing further reduced the pressure in the test capsule from 4.1 to approximately 1.4 kPa (0.6 to ~0.2 psia). A steady-state pressure condition was reached at, or before, 2.5 s, providing about 0.5 s of steady-state operation before shutdown.

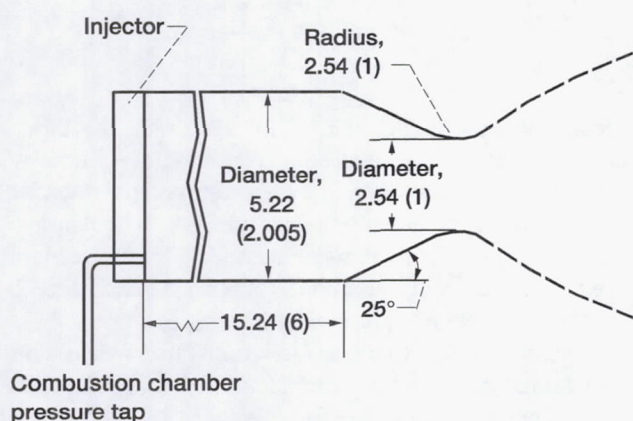


Figure 4.—Combustion chamber shape. For nozzle contour, see figure 6. Dimensions are in centimeters (in.).

Axial distance from throat		Radius	
cm	in.	cm	in.
0	0	1.2700	0.5000
.3929	.1547	1.4371	.5658
.4641	.1827	1.4961	.5890
.6068	.2389	1.6190	.6374
.7503	.2954	1.7404	.6852
.8230	.3240	1.8031	.7099
1.3246	.5215	2.2426	.8829
1.7844	.7025	2.6515	1.0438
2.3777	.9361	3.1643	1.2458
3.2062	1.2623	3.8572	1.5186
7.0256	2.7660	6.6703	2.6261
7.8931	3.1075	7.2426	2.8514
9.6269	3.7901	8.3320	3.2803
10.6505	4.1931	8.9433	3.5210
11.6738	4.5960	9.5341	3.7536
12.9022	5.0796	10.2189	4.0232
15.3429	6.0405	11.5108	4.5318
16.5392	6.5115	12.1150	4.7697
19.5651	7.7028	13.5702	5.3426
23.3688	9.2003	15.2710	6.0122
25.4869	10.0342	16.1651	6.3642
29.5410	11.6303	17.7871	7.0028
33.7297	13.2794	19.3558	7.6204
36.2996	14.2912	20.2705	7.9805
38.8696	15.3030	21.1524	8.3277
41.4193	16.3068	21.9977	8.6605
47.2194	18.5903	23.8201	9.3780
51.1703	20.1458	24.9895	9.8384
55.1213	21.7013	26.1064	10.2781
60.4944	23.8167	27.5486	10.8459
71.1091	27.9957	30.1694	11.8777
76.2211	30.0083	31.3365	12.3372
90.6396	35.6849	34.3444	13.5214
105.3071	41.3532	36.9933	14.5643
113.0838	44.5212	38.3365	15.0931
128.5725	50.6191	40.6598	16.0078

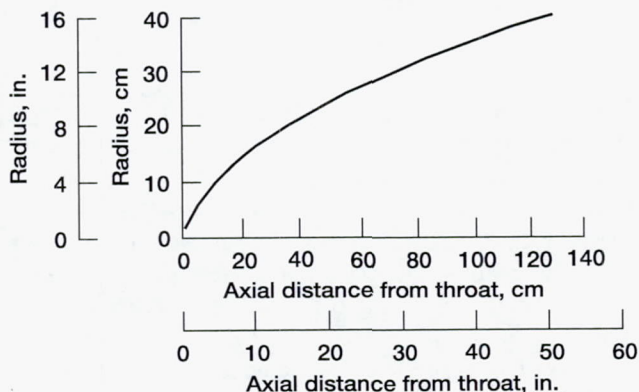


Figure 6.—Nozzle contour and coordinates.

At thruster shutdown, the exhaust flow through the diffuser stopped, and a pressure pulse propagated from the spray cooler to the test capsule, raising its pressure to the original 4.1 kPa (0.6 psia). Simultaneously, two isolation valves between the ejectors and the spray cooler were closed and the ejectors turned off.

Data Analysis

When experimental rocket results are described, three parameters need to be determined to characterize the performance and ascertain the magnitudes of the various losses: characteristic exhaust velocity C^* , the vacuum thrust coefficient $C_{F,V}$, and the vacuum specific impulse $I_{sp,V}$. To determine these, three test parameters were measured or derived: propellant mass flow \dot{m} , vacuum thrust F_V , and effective chamber pressure $P_{c,e}$.

Propellant Mass Flow

Propellant mass flows were measured with venturis. Each mass flow was calculated from conditions at the venturi throat by

$$\dot{m} = C_d \rho A_v V \quad (1)$$

where C_d is the venturi discharge coefficient, ρ is the throat density, A_v is the venturi throat area, and V is the velocity; ρ and V were calculated from one-dimensional mass and energy equations and real fluid properties were calculated from the fluid properties program GASP (ref. 8). Venturi calibrations of C_d were performed by the Colorado Engineering Experiment Station. Values of the discharge coefficient are traceable to the National Institute of Standards and Technology, and the uncertainty values are ± 0.5 percent of full scale.

Vacuum Thrust

Vacuum thrust was determined by measuring the thrust produced at the test capsule ambient pressure P_a and by applying two corrections. The first correction compensated for the thrust-stand zero shift that occurred from the change in capsule pressure during thruster startup. This correction, referred to as an aneroid correction, is explained in reference 2. The second correction adjusted the thrust measured at a P_a of approximately 1.4 kPa (0.2 psia) to a thrust that would have been measured if P_a had been an absolute vacuum. This thrust was calculated by adding the force induced by the capsule pressure on the nozzle exit area to the measured thrust:

$$F_V = F + (P_a \times A_{ex}) \quad (2)$$

where F_V is the vacuum thrust (experimentally measured thrust corrected to vacuum conditions) and A_{ex} is the nozzle exit area.

Effective Chamber Pressure

To obtain a truly representative effective combustion chamber total pressure at the nozzle entrance $P_{c,e}$, a thorough survey of the distribution of pressures in the combustion chamber would have to be made by taking a reading on each of several static pressure taps in the combustion chamber. These measurements would then have to be integrated and averaged to obtain an integrated mean pressure that could then be corrected for momentum pressure loss and used as $P_{c,e}$. In an alternative method that was used for the present study, $P_{c,e}$ was determined by the equation

$$P_{c,e} = P_{c,a} \left(\frac{P_{c,T}}{P_{c,a}} \right) \left(\frac{P_{c,e}}{P_{c,T}} \right) \quad (3)$$

where $P_{c,a}$ is the chamber pressure measured at a single injector faceplate position, $P_{c,T}/P_{c,a}$ is the conversion of the chamber static pressure before combustion to total pressure after combustion (momentum pressure loss), and $P_{c,e}/P_{c,T}$ is the correction that accounts for any variations in pressure distribution across the injector face. The momentum pressure loss was calculated by the following equation from reference 9:

$$\frac{P_{c,T}}{P_{c,a}} = \left(\frac{P_s}{P_T} + \frac{I g_c - V_{av}}{C_{Th(ODE)}^* \epsilon_c} \right)^{-1} \quad (4)$$

where P_s/P_T is the static-to-total pressure ratio in the combustion chamber; I is the theoretical subsonic specific impulse inside the combustion chamber; g_c is the proportionality constant; V_{av} is the propellant mass-averaged injection velocity; $C_{Th(ODE)}^*$ is the theoretical characteristic exhaust velocity, and ϵ_c is the thruster contraction area ratio. The ratio $P_{c,e}/P_{c,T}$ was derived semiempirically by the following procedure. A series of low-area-ratio nozzle tests were performed to develop a correlation between single-point chamber pressure measurements corrected for momentum pressure loss and the effective chamber pressure. These two pressures are defined at the same axial location in the chamber and vary only in that $P_{c,T}$ defines a single point and $P_{c,e}$ defines an average pressure at that axial location. This procedure is a calibration of the injector and chamber pressure tap. In these tests, the contour of the combustion chamber up to the throat was identical to that used in the test of the high-area-ratio nozzles.

The contour downstream of the throat was identical to that of a low-area-ratio divergent nozzle with a thrust coefficient calculated by an iterative procedure from a well-validated nozzle performance code, in this case the 1994 revised Two-Dimensional-Kinetics (TDK) program (ref. 7). The calculated thrust coefficient obtained from TDK was used with the experimental measurements of thrust from the low-area-ratio tests and with a value of $P_{c,e}$ calculated by the following equation:

$$P_{c,e} = \frac{F_V}{C_{F,V,Th(TDK)} A_t} \quad (5)$$

where $C_{F,V,Th(TDK)}$ is the theoretical, two-dimensional-kinetics, vacuum thrust coefficient and A_t is the nozzle throat area. The values of $P_{c,e}$ were then related to the calculated total pressure after combustion $P_{c,T}$ and a correlation was developed. This correlation, $P_{c,e}/P_{c,T}$, was plotted versus the propellant mixture ratio O/F and represents the correction for nonuniform pressure distributions (fig. 7). A straight line was fit to the data with a least-squares best fit and the equation of this line was used as the correlation.

Because the same injector and chamber contour was used in both the low-area-ratio and high-area-ratio tests, equation (3) is valid. The chamber static pressure was measured at the injector face static tap to obtain $P_{c,a}$. The momentum pressure loss conversion (eq. (4)) provided a value of $P_{c,T}/P_{c,a}$. The semiempirical correlation $P_{c,e}/P_{c,T}$ versus O/F from the low-area-ratio nozzle tests provided the $P_{c,e}/P_{c,T}$ correlation.

Performance Calculations

By definition,

$$C^* = \frac{P_{c,e} A_t g_c}{\dot{m}} \quad (6)$$

$$C_{F,V} = \frac{F_V}{P_{c,e} A_t} \quad (7)$$

$$I_{sp,V} = \frac{F_V g_c}{\dot{m} g} \quad (8)$$

The values of $P_{c,e}$ were determined as described in the preceding section. The calculations of mass flow and vacuum thrust were also described in a previous section. The throat diameter was measured each test day to ensure that no distortion or eroding was occurring. None was observed and an average value was used to calculate the throat area. The throat areas are given in tables I and II; there is one value for each piece of hardware.

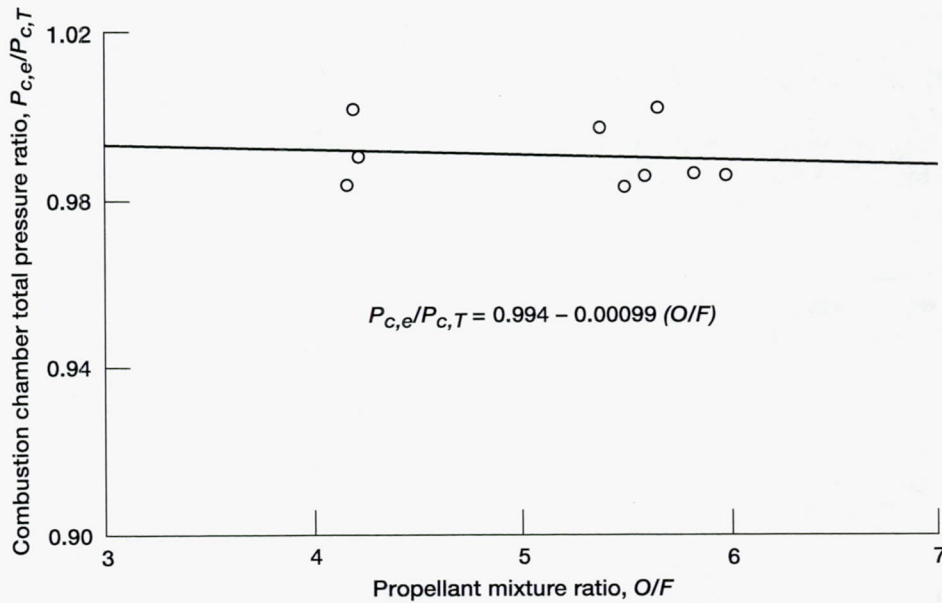


Figure 7.—Effective chamber pressure correlation.

Efficiency Calculations

The performance parameters ($I_{sp,V}$, $C_{F,V}$, C^*) were divided by theoretical, one-dimensional-equilibrium (ODE) values obtained from the Chemical Equilibrium Composition (CEC) program (ref. 6) to derive the efficiencies. The inlet enthalpy conditions were derived from measurements of the injection pressure and temperature of the hydrogen and oxygen. The equations for the various efficiencies follow. The characteristic exhaust velocity efficiency is

$$\eta_{C^*} = \frac{C^*}{C_{Th(ODE)}^*} \quad (9)$$

where $C_{Th(ODE)}^*$ is the theoretical, one-dimensional-equilibrium characteristic exhaust velocity. The vacuum thrust coefficient efficiency is

$$\eta_{C_{F,V}} = \frac{C_{F,V}}{C_{F,V,Th(ODE)}} \quad (10)$$

where $C_{F,V,Th(ODE)}$ is the theoretical, one-dimensional-equilibrium vacuum thrust coefficient. The vacuum specific impulse efficiency is

$$\eta_{I_{sp,V}} = \frac{I_{sp,V}}{I_{sp,V,Th(ODE)}} \quad (11)$$

Results and Discussion

Atmospheric Pressure Tests

Tests were performed at atmospheric pressure to determine the relationship between the effective and measured chamber pressures of the thruster. The tests were conducted with low-area-ratio configurations ($\epsilon = 10.7:1$ and $4:1$), the performance of which is well documented and agrees with calculated values from the TDK program. Because of the low area ratio of the nozzles, an altitude condition was not necessary for full unseparated flow. The results of the atmospheric tests are summarized in table I. Nine successful firings are listed between readings 514 and 530. In table I, the measured combustion chamber static pressure at the injector face is listed as $P_{c,a}$; the $P_{c,T}$ is derived from the $P_{c,a}$ values by using equation (4). The effective chamber pressures $P_{c,e}$, derived from thrust measurements as previously described, are also listed in table I. A consistent variation between $P_{c,e}$ and $P_{c,T}$

was observed and was attributed to variations in the static pressure profile that probably occurred at the static tap used for the $P_{c,a}$ measurements.

To properly account for the decrease in thrust attributable to combustion losses, C^* and ηC^* were derived for both the atmospheric and altitude tests. Within the range of these tests, chamber pressure had no effect on ηC^* and caused only a slight variation with respect to O/F . The ηC^* as a function of O/F is shown in figure 8 for all the atmospheric and altitude firings. A mean value of ηC^* was described by a second-order polynomial curve fit by the least-squares method, with values ranging from approximately 99.0 to 99.9 percent.

Altitude Tests

High-area-ratio nozzle tests were performed at altitude conditions to avoid separated flow in the divergent portion of the nozzle. The first objective of the tests was to ascertain whether the flow was attached or separated by examining the nozzle wall static pressure distribution. Static pressures were measured at eight axial locations and are given in table III. A typical distribution along the length of the nozzle is shown in figure 9. Plotted here from reading 577 is the static pressure ratio $P_s/P_{c,e}$ versus the nozzle expansion ratio of the pressure tap locations. The result is a straight line when plotted on log-log coordinates. If the flow were separated, the pressure

distribution would display a sudden increase. As this was not the case for any of the tests, all data reported are with attached flow.

Ten successful firings were accomplished at altitude, seven with the 1025:1-area-ratio nozzle and three with the nozzle truncated to an area ratio of 440:1. The results of these firings are summarized in table II. Listed are the measured values along with various calculated values.

The nozzle thrust performance is shown as the vacuum thrust coefficient in figure 10. Two sets of data are shown; the first is for the original nozzle with the 1025:1-area ratio, and the second is for the truncated nozzle with the 440:1-area ratio. Straight lines of the best fit by the least-squares method are shown. For the 1025:1 nozzle, the thrust coefficients ranged from approximately 1.92 to 2.02 and for the 440:1 nozzle, from 1.83 to 1.94.

The nozzle thrust efficiency is shown in figure 11. Straight lines of best fit by the least-squares method are shown. The efficiencies ranged from approximately 96.6 to 97.5 percent for the 1025:1-nozzle and from 94.0 to 94.2 percent for the 440:1-nozzle.

The overall thruster efficiency is shown in figure 12 in which specific impulse efficiency is plotted as a function of O/F for the 1025:1- and 440:1-area-ratio configurations. Each data point also agrees individually with

$$\eta C^* \times \eta C_{F,V} = \eta I_{sp,V} \quad (12)$$

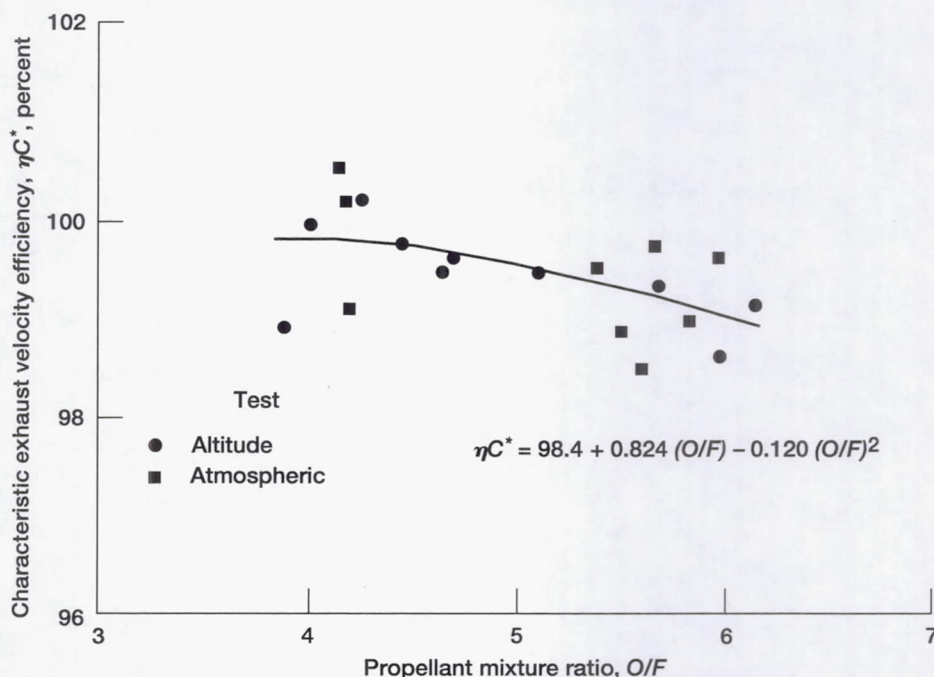


Figure 8.—Characteristic exhaust velocity efficiency as function of propellant mixture ratio.

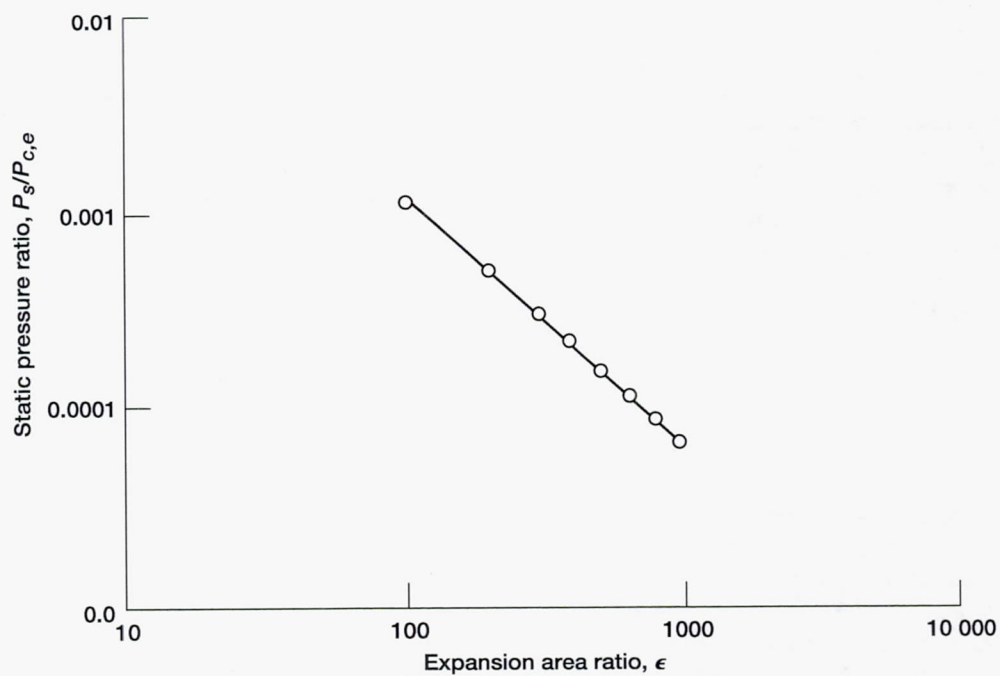


Figure 9.—Typical nozzle wall static pressure distribution (reading 577).

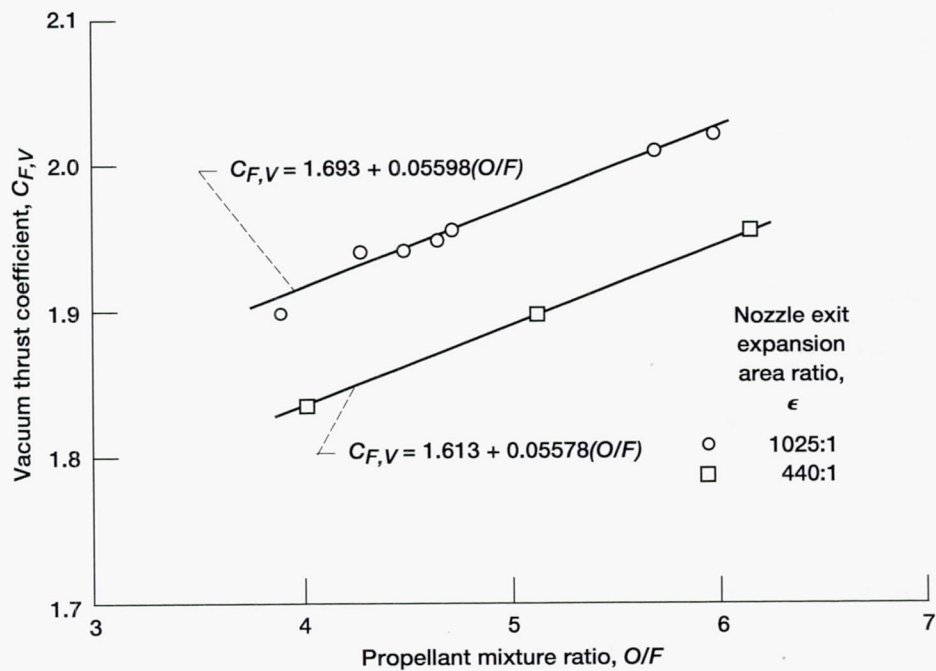


Figure 10.—Nozzle thrust performance.

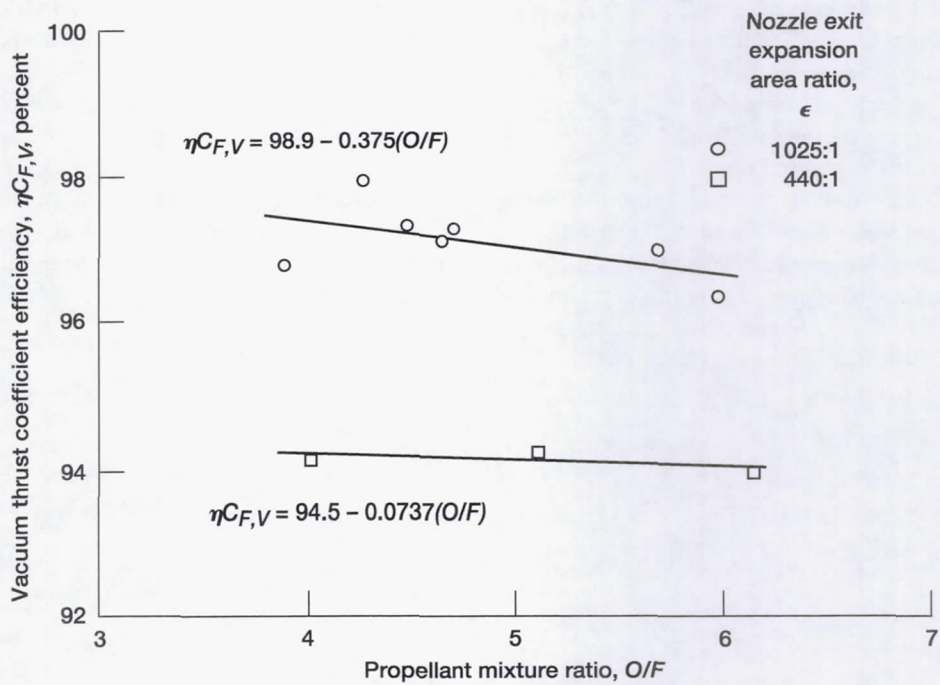


Figure 11.—Nozzle thrust efficiency.

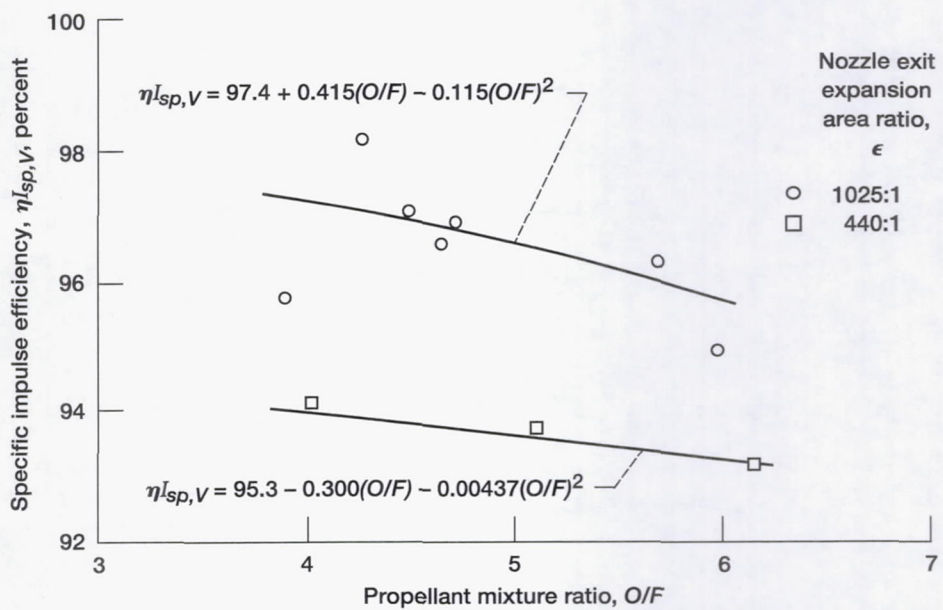


Figure 12.—Overall thruster efficiency.

The faired curves shown through the data were obtained from the product of the best-fit curves of ηC^* and $\eta C_{F,V}$ of figures 8 and 11. The coincidence of the faired curves through the center of the apparent data scatter reinforces the quality of the results. Values of $\eta I_{sp,V}$ ranged from 95.5 to 97.5 percent for the 1025:1-nozzle configuration and from 93.3 to 94.0 percent for the 440:1-nozzle configuration.

Figure 13 shows the overall thruster performance with a plot of specific impulse versus O/F for both the 1025:1- and 440:1-configurations. The faired curves were obtained from the product of the faired curves of figure 11 and the theoretical ODE values of reference 6. Again, the coincidence of the faired

values through the center of the apparent data scatter reinforces the quality of the data. The specific impulse attained was as high as 488 s for the 1025:1-nozzle configuration and 467 s for the 440:1-nozzle configuration.

Nozzle wall temperatures were measured at nine axial locations in a row circumferentially displaced 45° from the static pressure tap locations (table IV). The thermocouples spot welded to the outside surface of the nozzle read outside wall surface temperatures. Figure 14 shows a typical temperature distribution along the length of the nozzle for reading 577. These temperatures define the thermal boundary conditions of the nozzle flow.

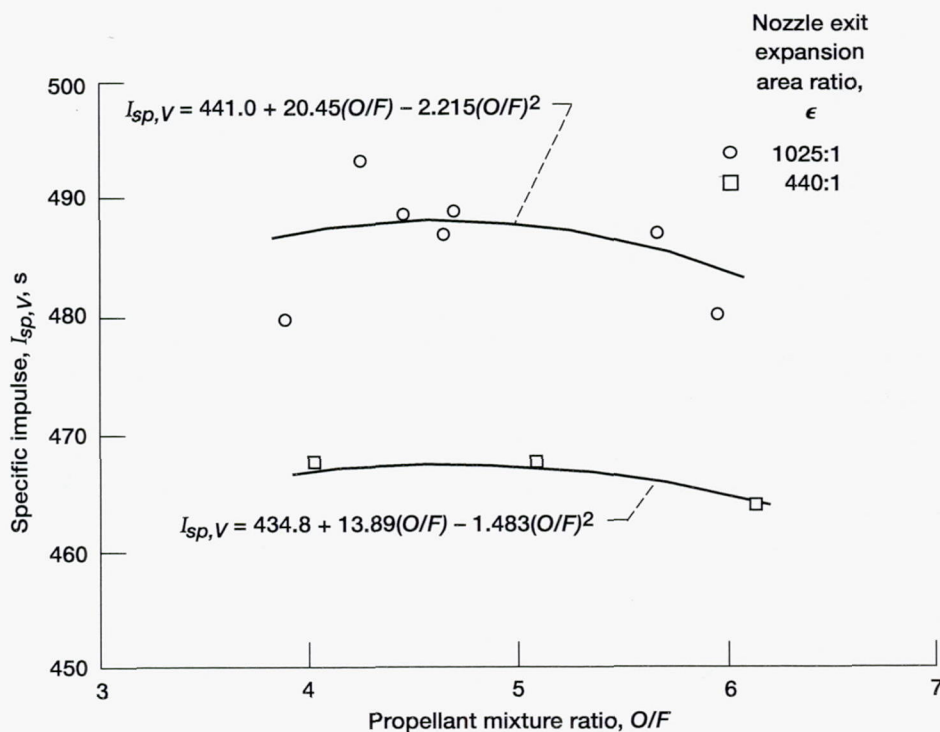


Figure 13.—Overall thruster performance.

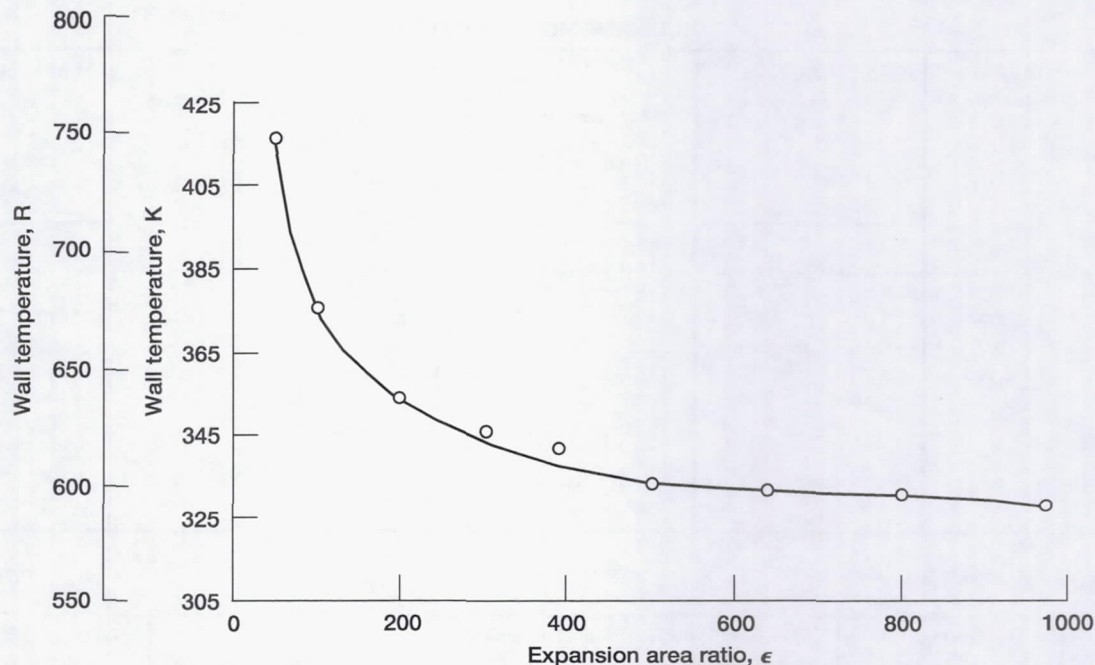


Figure 14.—Typical nozzle wall temperature distribution (reading 577).

Summary of Results

A series of high-pressure firings were conducted to experimentally measure the thrust coefficient of a high-area-ratio rocket nozzle operating at high combustion chamber pressures. The nozzle had an expansion area ratio of 1025:1 and a throat diameter of 2.54 cm (1 in.). The tests were performed in the altitude test capsule at the Rocket Engine Test Facility of the NASA Lewis Research Center. The propellants were gaseous hydrogen and liquid oxygen and the combustion chamber pressures ranged from 12.4 to 16.5 MPa (1800 to 2400 psia). Combustion losses and nozzle losses were precisely separated by a rigorous procedure for determining the effective chamber pressure. Characteristic exhaust velocity efficiency, nozzle thrust coefficient, and thruster specific impulse were determined. The parameter of primary concern, the nozzle vacuum thrust coefficient for the 1025:1-nozzle, ranged from 1.92 to 2.02 over the range of chamber pressures and mixture ratios tested.

Acknowledgments

The authors wish to acknowledge the efforts of Doug Bewley and Tom Soldat. The quality of data is evidence of their commitment to excellence and attention to detail.

Lewis Research Center
National Aeronautics and Space Administration
Cleveland, Ohio, October 12, 1995

References

1. Coats, D.E.; Berker, D.R.; and Dunn, S.S.: Boundary Layer Study. Software and Engineering Associates, Inc., Carson City, NV, 1990.
2. Pavli, A.J., et al.: Experimental Thrust Performance of a High-Area-Ratio Rocket Nozzle. NASA TP-2720, 1987.
3. Kacynski, K.J.; Pavli, A.J.; and Smith, T.A.: Experimental Evaluation of Heat Transfer on a 1030:1 Area Ratio Rocket Nozzle. AIAA Paper 87-2070 (NASA TP-2726), 1987.
4. Smith, T.A.; Pavli, A.J.; and Kacynski, K.J.: Comparison of Theoretical and Experimental Thrust Performance of a 1030:1 Area Ratio Rocket Nozzle at a Chamber Pressure of 2413 kN/m² (350 psia). AIAA Paper 87-2069 (NASA TP-2725), 1987.
5. Schoenman, L.: Low-Thrust ISP Sensitivity Study. (NASA Contract NAS 3-22665) NASA CR-165621, 1982.
6. Gordon, S.; and McBride, B.J.: Computer Program for Calculation of Complex Chemical Equilibrium Compositions, Rocket Performance, Incident and Reflected Shocks, and Champman-Jouguet Detonations. NASA SP-273, 1971.
7. Two-Dimensional Kinetics (TDK), Liquid Propellant Rocket Engine Performance Program (LPP) Version June 1994, Software and Engineering Associates, Inc., Carson City, NV, 1994.
8. Hendricks, R.C.; Baron, A.K.; and Peller, I.C.: GASP: A Computer Code for Calculating the Thermodynamic and Transport Properties for Ten Fluids: Parahydrogen, Helium, Neon, Methane, Nitrogen, Carbon Monoxide, Oxygen, Fluorine, Argon, and Carbon Dioxide—Enthalpy, Entropy, Thermal Conductivity, and Specific Heat. NASA TN-D-7808.
9. Huff, V.N.; Fortini, A.; and Gordon, S.: Theoretical Performance of JP-4 Fuel and Liquid Oxygen as a Rocket Propellant. NACA RM-E56D23, 1956.

TABLE I.—RESULTS OF ATMOSPHERIC PRESSURE TESTS

Reading	Expansion area ratio, ϵ	Nozzle throat area, A_t		Measured chamber pressure				Propellant mixture ratio, O/F	Measured thrust, F	
				At injector face, $P_{c,A}$		Corrected for momentum pressure loss, $P_{c,T}$				
		cm ²	in. ²	MPa	psia	MPa	psia		N	lb _f
514	10.72	5.103	0.7909	13.942	2022.1	13.893	2014.9	4.21	11 209	2520.0
515	10.72	5.103	.7909	15.801	2291.7	15.748	2284.0	4.16	12 677	2850.1
523	3.99	5.091	.7890	12.254	1777.3	12.211	1771.0	4.19	9 491	2133.7
524	3.99	5.091	.7890	12.524	1816.4	12.461	1807.3	5.38	9 735	2188.6
526	4.02	5.047	.7823	14.362	2083.0	14.293	2072.9	5.66	11 174	2512.2
527				14.746	2138.7	14.675	2128.4	5.60	11 285	2537.1
528	↓	↓	↓	15.096	2189.4	15.023	2178.8	5.50	11 511	2587.8
529	↓	↓	↓	12.825	1860.1	12.756	1850.1	5.83	9 808	2205.0
530	↓	↓	↓	14.642	2123.6	14.564	2112.3	5.98	11 423	2568.2

Reading	Vacuum thrust, ^a F_V		Propellant flow rate, \dot{m}		Fuel injection pressure, P_{fi}		Fuel injection temperature, T_{fi}		Oxidizer injection pressure, P_{oi}	
	N	lb _f	kg/s	lb _m /s	MPa	psia	K	R	MPa	psia
514	11 746	2640.7	2.852	6.287	17.818	2584.2	294.9	530.8	15.271	2214.8
515	13 214	2970.8	3.158	6.962	20.030	2905.0	294.7	530.4	17.411	2525.1
523	9 690	2178.5	2.500	5.512	16.147	2341.9	308.5	555.3	13.399	1943.3
524	9 934	2233.3	2.644	5.828	15.389	2231.9	306.5	551.7	13.891	2014.6
526	11 374	2557.0	3.037	6.696	17.508	2539.3	309.3	556.7	16.326	2367.8
527	11 486	2582.2	3.102	6.839	17.915	2598.3	300.8	541.5	16.791	2435.3
528	11 711	2632.8	3.143	6.928	18.258	2648.0	299.1	538.4	17.036	2470.8
529	10 008	2250.0	2.707	5.968	15.341	2224.9	299.8	539.6	14.329	2078.2
530	11 424	2568.3	3.082	6.794	17.420	2526.4	300.9	541.7	16.602	2407.8

^aMeasured thrust corrected to vacuum conditions.

TABLE I.—Concluded.

Reading	Oxidizer injection temperature, T_{oi}		Theoretically predicted			Effective chamber total pressure calculated from thrust, P_{ce}		Correlation pressure ratio for use in altitude tests, P_{ce}/P_{cT}	Characteristic exhaust velocity efficiency, ηC^* , percent
			ODE vacuum thrust coefficient, $C_{FV,Th(ODE)}$	TDK vacuum thrust coefficient, $C_{FV,Th(TDK)}$	Vacuum thrust coefficient efficiency, TDK/ODE ηC_{FV}				
	K	R				MPa	psia		
514	90.9	163.6	1.737	1.673	96.3	13.758	1995.4	0.990	99.1
515	88.8	159.9	1.736	1.673	96.4	15.483	2245.5	.983	100.6
523	96.7	174.1	1.601	1.557	97.2	12.230	1773.81	1.002	100.2
524	92.9	167.3	1.615	1.570	97.2	12.433	803.2	.998	99.5
526	110.2	198.3	1.619	1.573	97.2	14.327	2077.9	1.002	99.8
527	110.2	198.4	1.619	1.572	97.1	14.476	2099.5	.986	98.5
528	92.3	166.2	1.617	1.571	97.2	14.769	2142.01	.983	98.9
529	92.8	167.0	1.622	1.576	97.2	12.585	825.3	.987	99.0
530	93.1	167.6	1.623	1.576	97.1	14.365	2083.3	.986	99.6

Reading	Vacuum specific impulse $I_{sp,V}$, s	Vacuum specific impulse efficiency, $\eta I_{sp,V}$, percent	Ambient pressure around nozzle, P_a	
			kPa	psia
514	420.0	95.5	98.143	14.234
515	426.7	96.9	98.109	14.229
523	395.2	97.4		
524	383.2	96.7	↓	↓
526	381.9	96.9		
527	377.6	95.7	98.854	14.337
528	380.0	96.0	98.819	14.332
529	377.0	96.2	98.785	14.327
530	378.0	96.8	98.681	14.312

TABLE II.—RESULTS OF ALTITUDE PRESSURE TESTS

Reading	Nozzle throat area, A_t		Nozzle exit expansion area ratio, ϵ	Measured chamber pressure				Effective chamber pressure, ^a P_{ce}		Propellant mixture ratio, O/F
	cm ²	in. ²		At injector end, P_{ca}		Corrected for momentum pressure loss, $P_{c,T}$		MPa	psia	
				MPa	psia	MPa	psia			
569	5.067	0.7854	1025	12.485	1810.8	12.448	1805.3	12.326	1787.7	3.89
570	↓	↓	↓	12.867	1866.1	12.797	1856.0	12.645	1834.0	5.97
571				12.675	1838.3	12.621	1830.4	12.488	1811.1	4.70
575				14.562	2111.9	14.502	2103.3	14.350	2081.2	4.65
576				14.850	2153.8	14.775	2142.9	14.605	2118.2	5.68
577				14.429	2092.7	14.373	2084.6	14.225	2063.1	4.47
580				16.586	2405.5	16.531	2397.5	16.364	2373.3	4.27
601	5.007	.7760	440	12.993	1884.4	12.923	1874.3	12.768	1851.8	6.15
602	5.007	.7760	440	12.740	1847.7	12.681	1839.2	12.542	1819.0	5.11
603	5.007	.7760	440	12.621	1830.4	12.581	1824.7	12.457	1806.7	4.01

^aCalculated with low nozzle exit expansion area ratio ϵ correlation.

Reading	Vacuum thrust, F_V		Ambient pressure around nozzle, P_a		Characteristic exhaust velocity, C^*		Characteristic exhaust velocity efficiency, ηC^* , percent
	N	lbf	kPa	psia	m/s	ft/s	
569	11 863	2667.1	1.491	0.2162	2476	8124	98.9
570	12 957	2913.0	1.342	.1947	2330	7643	98.6
571	12 392	2785.9	1.313	.1905	2448	8033	99.7
575	14 179	3187.7	1.470	.2132	2448	8033	99.5
576	14 904	3350.8	1.510	.2190	2372	7782	99.4
577	14 010	3149.8	1.446	.2097	2467	8094	99.8
580	16 109	3621.7	1.582	.2295	2490	8170	100.2
601	12 498	2809.7	.9143	.1326	2328	7637	99.2
602	11 923	2680.5	.7812	.1133	2416	7925	99.5
603	11 450	2574.1	.6943	.1007	2497	8192	100.0

TABLE II.—Concluded.

Reading	Fuel injection				Oxidizer injection				Propellant flow rate, \dot{m}	
	Pressure, P_{fi}		Temperature, T_{fi}		Pressure, P_{oi}		Temperature, T_{oi}			
	MPa	psia	K	R	MPa	psia	K	R	kg/s	l b _m /s
569	16.563	2402.2	297.1	534.8	13.509	1959.3	112.6	202.6	2.522	5.561
570	15.316	2221.3	297.1	534.8	14.393	2087.4	117.8	212.1	2.751	6.064
571	15.863	2300.7	297.3	535.1	13.967	2025.6	121.6	218.8	2.584	5.697
575	18.317	2656.6	296.3	533.3	16.138	2340.6	108.6	195.4	2.970	6.547
576	17.837	2586.9	296.8	534.2	16.778	2433.3	111.6	200.9	3.120	6.878
577	18.353	2661.8	296.8	534.3	15.998	2320.3	115.0	207.0	2.922	6.441
580	21.422	3106.9	298.9	538.1	18.521	2686.1	106.6	191.8	3.329	7.340
601	15.311	2220.6	300.7	541.3	14.480	2100.1	109.1	196.3	2.746	6.054
602	15.570	2258.2	299.5	539.1	14.011	2032.1	109.6	197.2	2.600	5.731
603	16.431	2383.1	299.3	538.8	13.707	1987.9	113.0	203.4	2.498	5.506

Reading	Measured vacuum thrust coefficient, C_{FV}	Thrust coefficient efficiency, ηC_{FV} , percent	Vacuum specific impulse, $I_{sp,V}$, s	Vacuum specific impulse efficiency, $\eta I_{sp,V}$, percent
569	1.900	96.8	479.6	95.8
570	2.022	96.3	480.4	95.0
571	1.958	97.3	489.0	96.9
575	1.950	97.1	486.9	96.9
576	2.014	97.0	487.2	96.4
577	1.944	97.3	489.0	97.1
580	1.943	97.9	493.4	98.2
601	1.955	94.0	464.1	93.2
602	1.899	94.2	467.7	93.7
603	1.836	94.2	467.5	94.1

TABLE III.—NOZZLE WALL STATIC PRESSURES

Reading	Effective combustion chamber total pressure at nozzle entrance, P_{ce}		Propellant mixture ratio, O/F	Expansion area ratio, ϵ					
				100		101.2		200	
	Nozzle wall static pressure, P_s								
	MPa	psia		kPa	psia	kPa	psia	kPa	psia
569	12.326	1787.7	3.89	13.34	1.935	---	---	5.766	0.8362
570	12.645	1834.0	5.97	14.39	2.087	---	---	6.281	.9109
571	12.488	1811.1	4.70	14.90	2.161	---	---	6.470	.9383
575	14.350	2081.2	4.65	17.03	2.470	---	---	7.350	1.066
576	14.605	2118.2	5.68	17.20	2.495	---	---	7.426	1.077
577	14.225	2063.1	4.47	16.80	2.436	---	---	7.302	1.059
580	16.364	2373.3	4.27	19.09	2.769	---	---	8.253	1.197
601	12.768	1851.8	6.15	---	---	14.78	2.143	---	---
602	12.542	1819.0	5.11	---	---	14.79	2.145	---	---
603	12.457	1806.7	4.01	---	---	13.68	1.984	---	---

Reading	Expansion area ratio, ϵ									
	202.4		300		303.6		388		392.7	
	Nozzle wall static pressure, P_s									
	kPa	psia	kPa	psia	kPa	psia	kPa	psia	kPa	psia
569	---	----	3.476	0.5041	---	----	2.522	0.3658	---	----
570	---	----	3.929	.5699	---	----	2.990	.4337	---	----
571	---	----	3.895	.5649	---	----	2.832	.4108	---	----
575	---	----	4.456	.6462	---	----	3.252	.4717	---	----
576	---	----	4.656	.6753	---	----	3.512	.5093	---	----
577	---	----	4.410	.6396	---	----	3.232	.4688	---	----
580	---	----	4.955	.7186	---	----	3.609	.5234	---	----
601	6.847	0.9930	---	----	4.028	0.5842	---	----	3.026	0.4389
602	6.723	.9750	---	----	4.003	.5805	---	----	2.968	.4305
603	6.172	.8952	---	----	3.725	.5403	---	----	2.755	.3996

TABLE III.—Concluded.

Reading	Expansion area ratio, ϵ							
	500		635		800		975	
	Nozzle wall static pressure, P_s							
	kPa	psia	kPa	psia	kPa	psia	kPa	psia
569	1.789	0.2594	1.351	0.1959	1.008	0.1462	0.7853	0.1139
570	2.224	.3225	1.624	.2356	1.197	.1736	.9163	.1329
571	2.035	.2952	1.496	.2169	1.105	.1602	.8550	.1240
575	2.299	.3335	1.687	.2446	1.247	.1809	.9646	.1399
576	2.535	.3676	1.854	.2689	1.362	.1975	1.048	.1520
577	2.289	.3320	1.674	.2428	1.246	.1807	.9550	.1385
580	2.549	.3697	1.872	.2715	1.380	.2002	1.069	.1551
601	---	----	---	----	---	----	----	----
602	---	----	---	----	---	----	----	----
603	---	----	---	----	---	----	----	----

TABLE IV.—NOZZLE WALL TEMPERATURES

Reading	Effective combustion chamber total pressure at nozzle entrance, $P_{c,e}$		Propellant mixture ratio, O/F	Expansion area ratio, ϵ					
				50		50.6		100	
	MPa	psia		Nozzle wall temperature					
				K	R	K	R	K	R
569	12.326	1787.7	3.89	361.69	651.05	-----	-----	325.56	586.00
570	12.645	1834.0	5.97	428.94	772.09	-----	-----	370.09	666.17
571	12.488	1811.1	4.70	411.62	740.91	-----	-----	363.23	653.82
575	14.350	2081.2	4.65	414.72	746.50	-----	-----	356.46	641.63
576	14.605	2118.2	5.68	438.81	789.86	-----	-----	379.98	683.96
577	14.225	2063.1	4.47	416.22	749.20	-----	-----	375.08	675.15
580	16.364	2373.3	4.27	429.66	773.38	-----	-----	366.32	659.37
601	12.768	1851.8	6.15	-----	-----	416.91	750.44	-----	-----
602	12.542	1819.0	5.11	-----	-----	421.42	758.56	-----	-----
603	12.457	1806.7	4.01	-----	-----	406.07	730.93	-----	-----

Reading	Expansion area ratio, ϵ									
	101.2		200		202.4		300		303.6	
	Nozzle wall temperature									
	K	R	K	R	K	R	K	R	K	R
569	----	----	306.32	551.38	----	----	299.35	538.83	----	----
570	----	----	339.28	610.71	----	----	327.02	588.63	----	----
571	----	----	337.71	607.88	----	----	327.87	590.16	----	----
575	----	----	324.02	583.23	----	----	311.82	561.27	----	----
576	----	----	348.91	628.03	----	----	335.87	604.57	----	----
577	----	----	353.87	636.96	----	----	345.15	621.27	----	----
580	----	----	330.98	595.76	----	----	317.27	571.08	----	----
601	365.07	657.13	----	----	328.47	581.25	----	----	317.13	570.84
602	391.28	704.31	----	----	365.24	657.44	----	----	350.88	631.58
603	382.32	688.18	----	----	367.27	661.08	----	----	358.88	645.99

TABLE IV.—Concluded.

Reading	Expansion area ratio, ε											
	388		392.7		500		635		800		975	
	Nozzle wall temperature											
	K	R	K	R	K	R	K	R	K	R	K	R
569	300.61	541.09	----	----	297.56	535.61	301.44	542.60	303.82	546.88	302.86	545.14
570	322.01	579.61	----	----	316.16	569.09	314.66	566.38	313.57	564.42	309.35	556.83
571	324.53	584.16	----	----	319.16	574.49	319.45	575.01	320.53	576.95	317.96	572.32
575	309.96	557.92	----	----	303.44	546.20	304.79	548.62	304.29	547.73	304.32	547.77
576	331.11	595.99	----	----	323.84	582.92	320.29	576.52	318.52	573.34	314.78	566.61
577	342.49	616.49	----	----	333.86	600.95	332.06	597.70	330.83	595.50	328.28	590.90
580	313.56	564.40	----	----	307.35	553.23	308.32	554.98	306.74	552.13	307.64	553.75
601	----	----	316.88	570.38	----	----	----	----	----	----	----	----
602	----	----	347.11	624.80	----	----	----	----	----	----	----	----
603	----	----	358.74	645.74	----	----	----	----	----	----	----	----

REPORT DOCUMENTATION PAGE			Form Approved OMB No. 0704-0188	
Public reporting burden for this collection of information is estimated to average 1 hour per response, including the time for reviewing instructions, searching existing data sources, gathering and maintaining the data needed, and completing and reviewing the collection of information. Send comments regarding this burden estimate or any other aspect of this collection of information, including suggestions for reducing this burden, to Washington Headquarters Services, Directorate for Information Operations and Reports, 1215 Jefferson Davis Highway, Suite 1204, Arlington, VA 22202-4302, and to the Office of Management and Budget, Paperwork Reduction Project (0704-0188), Washington, DC 20503.				
1. AGENCY USE ONLY (Leave blank)	2. REPORT DATE June 1996	3. REPORT TYPE AND DATES COVERED Technical Paper		
4. TITLE AND SUBTITLE Experimental Performance of a High-Area-Ratio Rocket Nozzle at High Combustion Chamber Pressure		5. FUNDING NUMBERS WU-506-42-72		
6. AUTHOR(S) Robert S. Jankovsky, John M. Kazaroff, and Albert J. Pavli				
7. PERFORMING ORGANIZATION NAME(S) AND ADDRESS(ES) National Aeronautics and Space Administration Lewis Research Center Cleveland, Ohio 44135-3191		8. PERFORMING ORGANIZATION REPORT NUMBER E-9849		
9. SPONSORING/MONITORING AGENCY NAME(S) AND ADDRESS(ES) National Aeronautics and Space Administration Washington, D.C. 20546-0001		10. SPONSORING/MONITORING AGENCY REPORT NUMBER NASA TP-3576		
11. SUPPLEMENTARY NOTES Robert S. Jankovsky and John M. Kazaroff, NASA Lewis Research Center; Albert J. Pavli, NYMA, Inc., 2001 Aerospace Parkway, Brook Park, Ohio 44142 (work funded by NASA Contract NAS3-27186). Responsible person, Robert S. Jankovsky, organization code 5320, (216) 977-7515.				
12a. DISTRIBUTION/AVAILABILITY STATEMENT Unclassified - Unlimited Subject Category 20 This publication is available from the NASA Center for Aerospace Information, (301) 621-0390.		12b. DISTRIBUTION CODE		
13. ABSTRACT (Maximum 200 words) An experimental investigation was conducted to determine the thrust coefficient of a high-area-ratio rocket nozzle at combustion chamber pressures of 12.4 to 16.5 MPa (1800 to 2400 psia). A nozzle with a modified Rao contour and an expansion area ratio of 1025:1 was tested with hydrogen and oxygen at altitude conditions. The same nozzle, truncated to an area ratio of 440:1, was also tested. Values of thrust coefficient are presented along with characteristic exhaust velocity efficiencies, nozzle wall temperatures, and overall thruster specific impulse.				
14. SUBJECT TERMS High area ratio; Nozzle; Performance		15. NUMBER OF PAGES 24		
		16. PRICE CODE A03		
17. SECURITY CLASSIFICATION OF REPORT Unclassified	18. SECURITY CLASSIFICATION OF THIS PAGE Unclassified	19. SECURITY CLASSIFICATION OF ABSTRACT Unclassified	20. LIMITATION OF ABSTRACT	